

Application of Hierarchical TSO-DSO Coordination in European Pilot Projects

Zejun Ruan, Dimitris I. Chatzigiannis and Anthony Papavasiliou
National Technical University of Athens
Athens, Greece

Abstract—In this paper we present a hierarchical TSO-DSO coordination model that is suitable for short-term operations and requires minimal exchange of information between the Transmission (TSOs) and Distribution System Operators (DSOs). The proposed platform focuses on the balancing/real-time market, and its effectiveness is showcased on three real-world distribution systems, which were provided in the context of the FEVER research project in Germany and Spain.

Index Terms—Transmission System Operator (TSO), Distribution System Operator (DSO), TSO-DSO coordination, flexibility markets, balancing markets, congestion management, optimal power flow.

I. INTRODUCTION

In recent years, global power systems are transitioning towards decarbonized, clean and more efficient energy generation and consumption mechanisms through the increased integration of renewable generation at both high voltage (transmission) and medium/low voltage (distribution) levels [1]. This vast integration of distributed renewable generators and controllable loads, in short distributed energy resources (DERs), in the medium- and low-voltage distribution systems brings flexibility but also high uncertainty to the network, which results in greater needs for services from both TSO and DSO and creates conflicts and inefficiencies, if not coordinated. While TSOs use DERs for efficient system balancing for both transmission and distribution grids and congestion management, DSOs might potentially need the same resources for congestion management, voltage control and balancing at the distribution level. This implies that proper coordination between TSOs-DSOs and a well-designed market structure are necessary [2]–[4], and this issue has generated interest among the academic community and industry practitioners, leading to the development and implementation of advanced platforms for harnessing the flexibility of these resources and coordinating service providers with system operators. Such platforms aim at resolving balancing and congestion management issues, while also enabling the optimal coordination of transmission and distribution systems.

In this paper, a hierarchical scheme for the coordination of transmission and distribution system operations is proposed, which is inspired by nested decomposition and is suitable for integration in European balancing markets [5].

Our hierarchical approach aims at bridging the gap between the physical details of the grid constraints (that include the DSO grid) and the real-time market, operated by the TSO, which typically ignores most of the (DSO) grid constraints and underlying resources, notably for institutional reasons. In brief, the approach consists of implicitly representing DSO grid constraints and flexibility in the form of “grid-secure” bids (later called a residual supply function) that are submitted to the TSO balancing market through Residual Supply Functions (RSFs).

A. Contribution

Our work builds upon the deliverables of the EU Horizon 2020 FEVER project [6], which focused on the development of solutions and innovative services related to flexibility aggregation and management and the design of novel flexibility market mechanisms.

Real-time data derived from services developed in the project, as well as realistic network topology data, were provided from pilot participants and members of the consortium. This data was tested in our TSO-DSO coordination platform to simulate the operation of a real-time energy market. This is in contrast to the results presented in [5], which were based on test case systems that were the outcome of the EU Horizon 2020 SmartNet [7] project, where the focus was purely on models of Spanish and Italian systems, but without actual physical distribution networks being tested. As such, the results presented in this paper validate the application of the developed TSO-DSO coordination methodology in real-world distribution systems.

II. PLATFORM DESCRIPTION

In this section, a brief description of our proposed TSO-DSO coordination scheme is presented. For a more analytical approach the authors refer the reader to [5].

A. The Proposed Hierarchical Scheme

The developed hierarchical model aims to cover in real time the net load in both the Transmission and Distribution network. In this direction and in order to ensure the minimum amount of information exchange, the DSO calculates for each one of the examined distribution networks the implied Residual Supply Function (RSF), that constitutes the aggregated representation of the underlying flexibility, while fully respecting the network

constraints. The *RSF* is computed in N equally spaced points between the lower and upper flow limits of the interconnection and by solving an SOCP problem, the value of the RSF is derived. The derived RSFs from each Distribution Network are provided to the TSO, who incorporates them in the transmission-level market clearing problem and clears the real-time market. The outputs of this auction-based procedure are the clearing quantities of the participant orders, the market clearing prices and the power flow in the Transmission Network lines, which also contains the lines in the interface between the Transmission and the Distribution Networks.

The information regarding the optimal power flow that is cleared from or to the Distribution Network is then passed to the Distribution Network Operator, who incorporates it as a fixed injection in a power flow model, that derives the flexible resources' optimal dispatch schedules and the active and reactive market clearing prices. To avoid any line violations, the active and reactive power flows are limited by the distribution network line apparent power flow limits.

FSPs submit 15-minute upward or downward flexibility orders to the respective System Operators, whereas there is no specific requirement about the nominal size of the underlying bid [5].

B. Optimal Power Flow constraints

The *transmission network* that we consider is meshed, and we use a standard DC approximation (B-theta) which is considered adequate for high-voltage grids in market clearing models, while respecting line and generator capacity constraints.

Distribution networks are assumed to be radial in our model, and we consider AC power flow in order to account for losses, voltage limits, and reactive flows, which are more relevant in medium and low-voltage grids. Line constraints are also considered in this case. A quadratic relaxation is introduced [8], which is exact for radial networks and can be adapted easily for the second-order cone (SOC) relaxation [9].

The *interconnection* between the transmission and the distribution network is modeled with a lossless line. In case the losses of the interconnection need to be considered, the physical line can be included in the distribution network, and then an artificial lossless line can be introduced as the corresponding interconnection.

III. PRICING

In this section, we present an updated approach to the decentralized price calculation method introduced in [5]. The key idea is that after solving the primal dispatch model, according to [5], the dispatch decisions and all other primal variables of the master problem can be retrieved and then used to solve a linear system of the KKT equations that are associated with the distribution system (slave problem). This enables the retrieval of the distribution system's prices.

A. Distribution system monolithic

In the following section we present the distribution system formulation of the TSO-DSO coordination problem, where it is assumed that the distribution network is connected to a specific transmission node. We consider \mathcal{N} , \mathcal{E} as the set of distribution buses and the set of entities that provide active and reactive power. For operational and generation constraints, we introduce the sets \mathcal{OC}^{SOC} , \mathcal{GC}_g , respectively. The respective dual variables that are associated with each one of the primal problem constraints are highlighted in parentheses. The formulation of the monolithic is as follows:

$$\min \sum_{e \in \mathcal{E}} \sum_{b \in \mathcal{B}} \sum_{t \in \mathcal{T}} \left[P_{etb}^{up} \cdot p_{etb}^{up} - P_{etb}^{dn} \cdot p_{etb}^{dn} \right] \quad (1)$$

$$\begin{aligned} (p_{etb}^{up}, p_{etb}^{dn}, q_{et}^{up}, q_{et}^{dn}) \in \mathcal{GC}_g, \\ \forall g \in \mathcal{E} \quad (\beta_{etb}^{up}), (\beta_{etb}^{dn}), (\xi_{et}^{up}), (\xi_{et}^{dn}) \end{aligned} \quad (2)$$

$$F_i(x^D) = 0, \quad \forall i \in \mathcal{N} \quad (\lambda_{nt}^p), (\lambda_{nt}^q) \quad (3)$$

$$\begin{aligned} (c, s, f^p, f^q) \in \mathcal{OC}^{SOC} \quad (l_{nt}^{p/q}), (\gamma_{nn't}^{p/q}), (\kappa_{nn't}), (\sigma_{nn't}), \\ (v_{nt}^{min/max}), (\zeta_{nt}), (\delta_{nn't}^{c/s}) \end{aligned} \quad (4)$$

where the decision variables are $x_D = (p, q, c, s, f^p, f^q)$. Constraint (2) relates to the distribution generation constraints, constraint (3) describes the distribution real and reactive power balance and constraint (4) describes the operational distribution constraints. The detailed formulation of the model can be found in the Appendix B. The transmission system formulation follows that of [5].

B. Karush-Kuhn Tucker Equations

The KKT equations of the above-presented monolithic formulation are categorized in "types" following [10]. We denote with *hat* the primal variables that are fixed to their optimal value.

1) Type 1 constraints:

$$\text{All equality constraints of the original primal problem.} \quad (5)$$

2) Type 2 constraints: Contains all inequality constraints of the primal problem, that are complementary to one of the positive dual variables:

$$0 \leq \beta_{etb}^{up} \perp Q_{etb}^{up} - p_{etb}^{\hat{up}} \geq 0 \quad \forall e \in \mathcal{E}, t \in \mathcal{T}, b \in \mathcal{B} \quad (6)$$

$$0 \leq \beta_{etb}^{dn} \perp Q_{etb}^{dn} - p_{etb}^{\hat{dn}} \geq 0 \quad \forall e \in \mathcal{E}, t \in \mathcal{T}, b \in \mathcal{B} \quad (7)$$

$$0 \leq \xi_{et}^{up} \perp Q_e^{max} - q_{et}^{\hat{up}} \geq 0 \quad \forall e \in \mathcal{E}, t \in \mathcal{T} \quad (8)$$

$$0 \leq \xi_{et}^{dn} \perp Q_e^{min} - q_{et}^{\hat{dn}} \geq 0 \quad \forall e \in \mathcal{E}, t \in \mathcal{T} \quad (9)$$

$$0 \leq \kappa_{nn't} \perp (S_{nn'}^{max})^2 - (f_{nn't}^{\hat{p}})^2 - (f_{nn't}^{\hat{q}})^2 \geq 0 \quad \forall (n, n') \in \mathcal{L}, t \in \mathcal{T} \quad (10)$$

$$(p_{nt}^{inj}) : -\lambda_{nt}^p - l_{nt}^p = 0 \quad \forall n \in \mathcal{N}, t \in \mathcal{T} \quad (20)$$

$$0 \leq v_{nt}^{min} \perp -(V_n^{min})^2 + c_{\hat{n}nt} \geq 0 \quad \forall n \in \mathcal{N}, t \in \mathcal{T} \quad (11)$$

$$(q_{nt}^{inj}) : -\lambda_{nt}^q - l_{nt}^q = 0 \quad \forall n \in \mathcal{N}, t \in \mathcal{T} \quad (21)$$

$$0 \leq v_{nt}^{max} \perp (V_n^{max})^2 - c_{\hat{n}nt} \geq 0 \quad \forall n \in \mathcal{N}, t \in \mathcal{T} \quad (12)$$

$$(f_{nn't}^p) : l_{nt}^p - \gamma_{nn't}^p + 2 \cdot \kappa_{nn't} \cdot f_{nn't}^{\hat{p}} = 0 \quad \forall (n, n') \in \mathcal{L}, t \in \mathcal{T} \quad (22)$$

$$0 \leq \sigma_{nn't} \perp c_{\hat{n}nt} \cdot c_{\hat{n}'n't} - (c_{\hat{n}n't})^2 - (s_{\hat{n}n't})^2 \geq 0 \quad \forall (n, n') \in \mathcal{L}, n \neq n', t \in \mathcal{T} \quad (13)$$

$$(f_{nn't}^q) : l_{nt}^q - \gamma_{nn't}^q + 2 \cdot \kappa_{nn't} \cdot f_{nn't}^{\hat{q}} = 0 \quad \forall (n, n') \in \mathcal{L}, t \in \mathcal{T} \quad (23)$$

3) Type 3 constraints: Constraints that are associated to the non-negative primal variables $c_{\hat{n}nt}$, p_{etb}^{up} , p_{etb}^{dn} , q_{et}^{up} , q_{et}^{dn} , that are complementary to dual inequality constraints.

$$(s_{nn't}) : \zeta_{nt} = 0 \quad \forall n \in \mathcal{N}, t \in \mathcal{T} \quad (24)$$

$$0 \leq p_{etb}^{\hat{up}} \perp P_{etb}^{up} + \beta_{etb}^{up} + \sum_{n \in \mathcal{N}} I_{en} \cdot \lambda_{nt}^p \geq 0 \quad \forall e \in \mathcal{E}, t \in \mathcal{T}, b \in \mathcal{B} \quad (14)$$

$$(s_{nn't}) : -B_{nn'} \cdot \gamma_{nn't}^p - G_{nn'} \cdot \gamma_{nn't}^q + 2 \cdot \sigma_{nn't} \cdot s_{\hat{n}n't} + \delta_{nn't}^s + \delta_{n'n't}^s = 0 \quad \forall (n, n') \in \mathcal{L}, t \in \mathcal{T} \quad (25)$$

$$0 \leq p_{etb}^{\hat{dn}} \perp -P_{etb}^{dn} + \beta_{etb}^{dn} - \sum_{n \in \mathcal{N}} I_{en} \cdot \lambda_{nt}^p \geq 0 \quad \forall e \in \mathcal{E}, t \in \mathcal{T}, b \in \mathcal{B} \quad (15)$$

By solving the above linear system (5)-(25) with respect to the primal variables of the monolithic distribution system model and additional information related to dual prices of the interface nodes of the transmission system, the distribution system's prices are obtained.

IV. PILOT DATASETS

$$0 \leq q_{et}^{\hat{up}} \perp \xi_{et}^{up} + \sum_{n \in \mathcal{N}} I_{en} \cdot \lambda_{nt}^q \geq 0 \quad \forall e \in \mathcal{E}, t \in \mathcal{T} \quad (16)$$

In this paper, the authors use data that were acquired in the context of the European-funded research project FEVER, for validating the TSO-DSO coordination model that was firstly presented in [5]. In the H2020 FEVER project the actual physical systems were modeled in pandapower format and additional feedback from pilot participants was required in order to implement the exact network topology of the pilots on the already developed TSO-DSO coordination platform. In addition to the network topology data and measurements of smart meters, which were implemented in the pilots, additional data regarding the quantity and pricing of the flex offers were provided in most cases.

The examined real-world distribution systems were presented in the [11] and [12] FEVER deliverables and are briefly presented below:

$$0 \leq q_{et}^{\hat{dn}} \perp \xi_{et}^{dn} - \sum_{n \in \mathcal{N}} I_{en} \cdot \lambda_{nt}^q \geq 0 \quad \forall e \in \mathcal{E}, t \in \mathcal{T} \quad (17)$$

$$0 \leq c_{\hat{n}nt} \perp \sum_{n' \in \mathcal{N}} (g_{nn'} + g_{nn'}^{sh}) \cdot \gamma_{nn't}^p - \sum_{n' \in \mathcal{N}} (b_{nn'} + b_{nn'}^{sh}) \cdot \gamma_{nn't}^q - v_{nt}^{min} + v_{nt}^{max} - \sum_{n' \in \mathcal{N}_n} \sigma_{nn'} \cdot c_{\hat{n}'n'} - \sum_{n' \in \mathcal{N}_n} \sigma_{n'n} \cdot c_{\hat{n}'n'} \geq 0, \quad \forall n \in \mathcal{N}, t \in \mathcal{T} \quad (18)$$

$$0 \leq c_{\hat{n}n't} \perp G_{nn'} \cdot \gamma_{nn't}^p - B_{nn'} \cdot \gamma_{nn't}^q + 2 \cdot c_{\hat{n}n't} \cdot \sigma_{nn't} + \delta_{nn't}^c - \delta_{n'n't}^c \geq 0, \quad \forall (n, n') \in \mathcal{L}, t \in \mathcal{T} \quad (19)$$

4) Type 4 constraint: Constraints that correspond to the dual equalities that are associated with the free primal variables p_{nt}^{inj} , q_{nt}^{inj} , $f_{nn't}^p$, $f_{nn't}^q$, $s_{nn't}$, $s_{nn't}$:

TABLE I
PILOT NETWORKS AFTER CONVERSIONS

Test Case	Estebanell	SWW	SWH
# Buses	223	21	24
# Edges	222	20	23
Country	Spain	Germany	Germany
Voltage range	220kV - 0.4kV	20kV - 0.4kV	110kV - 0.4kV
# Flex assets	5	4	3

A. Estebanell

The Spanish network consists of 224 buses, 223 edges, 110 loads and 3 distributed energy resources (DERs). DERs and loads are modeled as price-inelastic power withdrawals and injections respectively, and are thus not flexible in the real-time market. For the given case, 5 flexible assets were introduced to the Spanish distribution network.

For each Flexibility Service Provider, multiple flexible offers of variable duration, activation period and capacity were provided. One of the aforementioned offers had separate capacity for Winter and Summer operation, and the latter was selected due to the selected date of load measurements. In order to further simplify the examined test case, all flexible offers were assumed to be available for activation simultaneously, and thus an aggregated offer was created for each examined period, with a capacity equal to the total overall capacity of all provided offers for each FSP.

The upper and lower bus voltage limits were assumed to be equal to 0.95 pu and 1.05 pu respectively, as no alternative information was provided from the various data sources.

B. SWW

The German distribution network SWW consists of 22 buses, 21 edges, 23 loads and 9 DERs. For the examined case, 4 flexible assets were included in the network.

Due to the lack of information regarding the provided measurements of loads and DERs and the fact that the examined flex offers were given for four 15-minute intervals, it was assumed that each one of the provided measurement values corresponds to the respective 15-minute timeframe and remains the same for all the 4 examined periods.

Moreover, since we did not have any indication about the location where each flex offers was submitted, the respective distribution nodes were arbitrarily chosen. Finally, it was also assumed, as in the case of the Estebanell distribution network, that the upper and lower voltage limits were also 1.05 pu and 0.95 pu.

C. SWH

The German distribution network SWH comprises 25 buses, 24 edges (in the provided data 27 edges exist but three duplicate lines were merged), 16 loads and 16 DERs. For the examined case, 3 flexible assets were introduced in the network, the location of which was not disclosed and as such was selected arbitrarily.

In order to create nodal net injections for the SWH case, it was assumed that all load and generation data corresponded to the 15-minute interval measurements, instead of the original provided hourly interval. Moreover, the provided flexible offers comprised more than four 15-minute intervals. Since the optimization horizon is assumed to be equal to 1 hour in all pilot test cases, only the first four time intervals were processed and used in the simulations. Additionally, the voltage limit assumptions of the Spanish Pilot were also adopted in the SWH network.

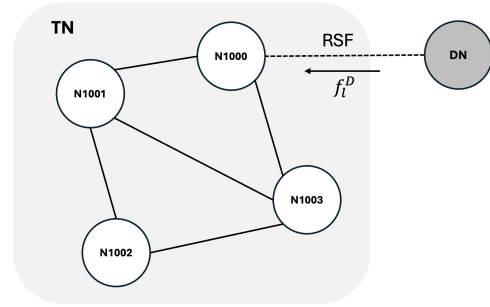


Fig. 1. Transmission network used in all case studies.

Finally, it should be noted that in all three cases, it was assumed that there exists a reactive bid of infinite capacity in the distribution network root node (that corresponds to the bus that is connected to the interface between the transmission and distribution networks), in order to ensure the feasibility of the power flow problem.

D. Transmission Network

In order to validate the proposed market clearing framework against the aforementioned real-world distribution networks, we used a simple 4-node transmission network, presented in Fig. 1.

In all examined cases, the distribution networks were connected to node N1000 and as such, the generated RSF curve was applied on the interconnecting line l , for deriving the optimal interface flow f_l^D . Moreover, arbitrary active power imbalances were assumed to exist in all examined periods in nodes N1002 and N1003, whereas upward/downward bids of adequate capacity and higher/lower price than the most expensive/cheap distribution network upward/downward bid were taken into consideration for transmission nodes N1001 and N1002.

It should be noted that, since the SWW and Estebanell distribution networks exhibit excess production, i.e. a long position, we primarily assumed short conditions in the corresponding transmission networks. In contrast to the two aforementioned cases, the SWH network represents the opposite scenario.

V. RESULTS

A. Performance Metrics

In order to validate the application of the proposed methodology on real-world systems, we utilize the Lost Opportunity Cost (LOC) performance metric, which measures the alignment of the market clearing solution with agent incentives. This metric is associated with the platform dispatch instructions and derived market clearing prices and highlights the financial loss that a participant incurs by following the platform dispatch instead of its own profit-maximizing actions.

Moreover, we compare the derived LOC with the Producer Load Payment (PLP) metric, which is calculated as the summation of the participants' revenues and payments, to provide

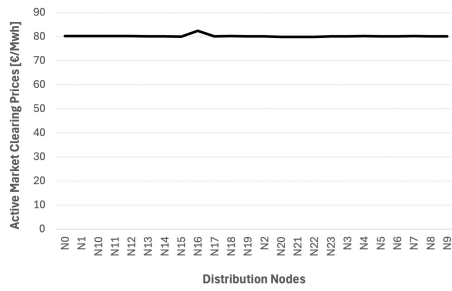


Fig. 2. Active distribution clearing prices for distribution network SWH and period T1.

a relative perspective on the derived LOC values in relation to the examined market depth [5].

B. Report Results

In the following subsection we present some indicative results from the application of the proposed TSO-DSO coordination methodology to the real-world distribution systems of SWH, SWW and Estebanell. In all cases, the submitted Residual Supply Function (RSF) was created using 1,000 points. For the sake of clarity we focus our analysis on the SWH test case system and we present comparative results to the other cases.

TABLE II
MARKET CLEARING PRICES IN PERIOD T1 [IN €/MWh]

N1000	N1001	N1002	N1003
82.42	68.57	27.00	96.28

In this case, after creating and submitting the RSF curve, the transmission network is cleared and the derived market clearing prices are presented in Table II, for the first examined period T1. Due to congestion in the transmission line between nodes N1002 and N1003, a price differentiation is observed between all nodes of the transmission network, whereas, the platform schedules an import of 0.286 MWh into the SWH distribution network. The active distribution prices for period T1 are presented in Fig. 2, highlighting that they follow the price of the interface transmission node N1000, due to uncongested interface and distribution lines.

TABLE III
LOST OPPORTUNITY COST

Test Case	LOC [€]	PLP [€]
SWH	$4 \cdot 10^{-5}$	18.92
SWW	$3 \cdot 10^{-4}$	14.96
Estebanell	$5 \cdot 10^{-3}$	10.96

Table III presents the total Lost Opportunity Cost of the non-network agents in the distribution network, for the three examined systems. In all cases the LOC is almost zero and negligible relative to the market PLP, validating the efficiency

of the proposed market clearing approach and indicating that the agents have no incentive to deviate from the platform dispatch instruction.

TABLE IV
TOTAL EXECUTION TIME [IN SECONDS]

Component	SWH	SWW	Estebanell
RSF Creation	43.27	38.71	992.66
TN Clearing	2.03	1.93	2.03
DN Clearing	2.13	2.36	3.23
Total Time	47.43	43.05	997.92

Finally, Table IV presents the execution time of each platform step. As observed, the most time consuming procedure is the creation of the RSF. It should be noted, though, that since each RSF point is calculated independently from the others, parallelization techniques may be employed to significantly reduce the overall execution time. Additional material is provided in [13].

VI. CONCLUSION & FURTHER RESEARCH

In this paper, the authors present the application of the real-time balancing and congestion management coordination methodology that was developed in [5] in three real-world distribution systems. The simulation results validate the proposed approach and showcase the balancing market clearing architecture on real-world power systems. In contrast to [5], an updated decentralized price calculation method is proposed, which solves a linear system of KKT equations to retrieve the distributional locational marginal prices.

Future research areas include the application of the proposed TSO-DSO coordination methodology in a large-scale test case system with a real-world transmission system and multiple distribution systems that are located in different high/medium voltage nodes.

ACKNOWLEDGMENT

This work was supported by the European Research Council (ERC) under the European Union's Horizon 2020 Research and Innovation Programme under Grant 850540, and by the H2020 FEVER Project under Grant 864537.

REFERENCES

- [1] J. Villar, R. Bessa, and M. Matos, "Flexibility products and markets: Literature review," pp. 329–340, 2018.
- [2] A. Vicente-Pastor, J. Nieto-Martin, D. W. Bunn, and A. Laur, "Evaluation of flexibility markets for retailer-dso-tso coordination," *IEEE Transactions on Power Systems*, vol. 34, pp. 2003–2012, 2019.
- [3] H. Gerard, E. I. R. Puente, and D. Six, "Coordination between transmission and distribution system operators in the electricity sector: A conceptual framework," *Utilities Policy*, vol. 50, pp. 40–48, 2 2018.
- [4] S. Y. Hadush and L. Meeus, "Dso-tso cooperation issues and solutions for distribution grid congestion management," *Energy Policy*, vol. 120, pp. 610–621, 9 2018.
- [5] I. Mezghani, N. Stevens, A. Papavasiliou, and D. I. Chatzigiannis, "Hierarchical coordination of transmission and distribution system operations in european balancing markets," *IEEE Transactions on Power Systems*, vol. 38, no. 5, pp. 3990–4002, 2023.

- [6] FEVER, “Flexible energy production, demand and storage-based virtual power plants for electricity markets and resilient dso operation,” 2020. [Online]. Available: <https://fever-h2020.eu/>
- [7] SmartNet, 2018. [Online]. Available: <https://smartnet-project.eu/>
- [8] R. Jabr, “Radial distribution load flow using conic programming,” *IEEE Transactions on Power Systems*, vol. 21, no. 3, pp. 1458–1459, 2006.
- [9] K. Burak, S. S. Dey, and X. A. Sun, “Strong SOCP Relaxations for the Optimal Power Flow Problem,” *Operations Research*, vol. 64, no. 6, pp. 1177–1196, 2016.
- [10] A. Papavasiliou, *Optimization Models in Electricity Markets*. Cambridge University Press, 2024.
- [11] FEVER, “Pilots’ validation report,” H2020 Project FEVER, Deliverable D7.3, Feb. 2024, [Online]. Available: https://fever-h2020.eu/data/deliverables/FEVER_D7.3_Pilots-validation-report.pdf [Accessed: Feb. 8, 2025].
- [12] FEVER, “Report on simulation tests with data from pilots,” H2020 Project FEVER, Deliverable D4.4, Jan. 2023, [Online]. Available: https://fever-h2020.eu/data/deliverables/FEVER_D4.4_Report-on-simulation-tests-with-data-from-pilots.pdf [Accessed: Feb. 8, 2025].
- [13] Z. Ruan, D. I. Chatzigiannis, and A. Papavasiliou, “Additional material: Application of Hierarchical TSO-DSO Coordination in European Pilot Projects,” 2025, [Online]. Available: https://ap-rg.eu/wp-content/uploads/2025/12/Application_of_Hierarchical_TSO_DSO_Coordination_in_European_Pilot_Projects_final.pdf [Accessed: Dec. 19, 2025].

APPENDIX

A. Nomenclature

The notation used in section III-A and Appendix B is analytically presented in Table V.

B. Distribution monolithic

In this section, we provide an analytical formulation of the distribution dispatch model used in section III-A. It should be noted that, for the sake of clarity, we introduce the F_{nt}^{IL} parameter to formulate the interface line active power injection into the distribution system root node, as this value was derived according to the methodology analytically presented in [5]. In all other nodes and examined periods, the respective parameter is equal to zero.

$$p_{etb}^{up} \leq Q_{etb}^{up} \quad \forall e \in \mathcal{E}, t \in \mathcal{T}, b \in \mathcal{B} \quad (\beta_{etb}^{up}) \quad (26)$$

$$p_{etb}^{dn} \leq Q_{etb}^{dn} \quad \forall e \in \mathcal{E}, t \in \mathcal{T}, b \in \mathcal{B} \quad (\beta_{etb}^{dn}) \quad (27)$$

$$q_{et}^{up} \leq Q_e^{max} \quad \forall e \in \mathcal{E}, t \in \mathcal{T} \quad (\xi_{et}^{up}) \quad (28)$$

$$q_{et}^{dn} \leq Q_e^{min} \quad \forall e \in \mathcal{E}, t \in \mathcal{T} \quad (\xi_{et}^{dn}) \quad (29)$$

$$\sum_{e \in \mathcal{E}} \sum_{b \in \mathcal{B}} I_{en} \cdot p_{etb}^{up} - \sum_{e \in \mathcal{E}} \sum_{b \in \mathcal{B}} I_{en} \cdot p_{etb}^{dn} + P_{nt}^{inj} + F_{nt}^{IL} - p_{nt}^{inj} = 0 \quad \forall n \in \mathcal{N}, t \in \mathcal{T} \quad (\lambda_{nt}^p) \quad (30)$$

$$\sum_{e \in \mathcal{E}} I_{en} \cdot q_{et}^{up} - \sum_{e \in \mathcal{E}} I_{en} \cdot q_{et}^{dn} + Q_{nt}^{inj} - q_{nt}^{inj} = 0 \quad \forall n \in \mathcal{N}, t \in \mathcal{T} \quad (\lambda_{nt}^q) \quad (31)$$

TABLE V
NOMENCLATURE

Symbol	Description
\mathcal{N}	Set of distribution nodes
\mathcal{N}_n	Subset of distribution nodes, denoting all nodes connected to distribution node n , $\mathcal{N}_n \subset \mathcal{N}$
\mathcal{L}	Set of bi-directional distribution lines between nodes (n, n')
\mathcal{E}	Set of entities providing active and reactive power
\mathcal{T}	Set of trading periods
\mathcal{B}	Set of upward or downward offer’s steps
$P_{etb}^{up/dn}$	Price of upward/downward active power, in €/MWh
$Q_{etb}^{up/dn}$	Quantity cap of upward/downward active power, in MW
$Q_e^{max/min}$	Reactive power capability limits of entity e , in MVar
P_{nt}^{inj}	Active power injection at node n , time t , in MW
Q_{nt}^{inj}	Reactive power injection at node n , time t , in MVar
F_{nt}^{IL}	Interface line flow directed at the distribution system root node n , time t , in MW
I_{en}	Incidence matrix denoting that entity e is connected to node n
$V_n^{max/min}$	Voltage magnitude limits at node n , in Volts
$S_{n,n'}^{max}$	Apparent power capacity of line (n, n') , in MVA
$G_{nn'}$	Conductance matrix, in pu
$B_{nn'}$	Susceptance matrix, in pu
$g_{nn'}, g_{nn'}^{sh}$	Line (n,n') conductance and shunt conductance, in pu
$b_{nn'}, b_{nn'}^{sh}$	Line (n,n') susceptance and shunt susceptance, in pu
p_{etb}^{up}	Upward active power offer from entity e at time t and bus b , in MW
p_{etb}^{dn}	Downward active power offer from entity e at time t and bus b , in MW
q_{et}^{up}	Upward reactive power offer from entity e at time t , in MVar
q_{et}^{dn}	Downward reactive power offer from entity e at time t , in MVar
p_{nt}^{inj}	Net active power injection (decision variable) at node n , time t , in MW
q_{nt}^{inj}	Net reactive power injection (decision variable) at node n , time t , in MVar
$f_{nn't}^p$	Active power flow on line (n, n') at time t , in MW
$f_{nn't}^q$	Reactive power flow on line (n, n') at time t , in MVar
$c_{nn't}$	Squared voltage product cosine term between n and n' , dimensionless
$s_{nn't}$	Sine component of voltage product between n and n' , dimensionless

$$\sum_{n' \in \mathcal{N}_n} f_{nn't}^p - p_{nt}^{inj} = 0 \quad \forall n \in \mathcal{N}, t \in \mathcal{T} \quad (l_{nt}^p) \quad (32)$$

$$\sum_{n' \in \mathcal{N}_n} f_{nn't}^q - q_{nt}^{inj} = 0 \quad \forall n \in \mathcal{N}, t \in \mathcal{T} \quad (l_{nt}^q) \quad (33)$$

$$(g_{nn'} + g_{nn'}^{sh}) \cdot c_{nnt} + G_{nn'} \cdot c_{nn't} - B_{nn'} \cdot s_{nn't} - f_{nn't}^p = 0 \quad \forall (n, n') \in \mathcal{L}, n \neq n', t \in \mathcal{T} \quad (\gamma_{nn't}^p) \quad (34)$$

$$\begin{aligned}
& -(b_{nn'} + b_{nn'}^{sh}) \cdot c_{nnt} - G_{nn'} \cdot s_{nn't} - B_{nn'} \cdot c_{nn't} \\
& - f_{nn't}^q = 0 \quad \forall (n, n') \in \mathcal{L}, n \neq n', t \in \mathcal{T} \quad (\gamma_{nn't}^q)
\end{aligned} \tag{35}$$

$$\begin{aligned}
& (f_{nn't}^p)^2 + (f_{nn't}^q)^2 \leq (S_{nn'}^{max})^2 \\
& \quad \forall (n, n') \in \mathcal{L}, n \neq n', t \in \mathcal{T} \quad (\kappa_{nn't})
\end{aligned} \tag{36}$$

$$-c_{nnt} \leq -(V_n^{min})^2 \quad \forall n \in \mathcal{N}, t \in \mathcal{T} \quad (v_{nt}^{min}) \tag{37}$$

$$c_{nnt} \leq (V_n^{max})^2 \quad \forall n \in \mathcal{N}, t \in \mathcal{T} \quad (v_{nt}^{max}) \tag{38}$$

$$\begin{aligned}
& (c_{nn't})^2 + (s_{nn't})^2 - c_{nnt} \cdot c_{n'n't} \leq 0 \\
& \quad \forall (n, n') \in \mathcal{L}^S, n \neq n', t \in \mathcal{T} \quad (\sigma_{nn't})
\end{aligned} \tag{39}$$

$$s_{nnt} = 0 \quad \forall n \in \mathcal{N}, t \in \mathcal{T} \quad (\zeta_{nt}) \tag{40}$$

$$c_{nn't} - c_{n'nt} = 0 \quad \forall (n, n') \in \mathcal{L}^S, n \neq n', t \in \mathcal{T} \quad (\delta_{nn't}^c) \tag{41}$$

$$s_{nn't} + s_{n'nt} = 0 \quad \forall (n, n') \in \mathcal{L}^S, n \neq n', t \in \mathcal{T} \quad (\delta_{nn't}^s) \tag{42}$$